PCCP

Accepted Manuscript

ROYAL SOCIETY OF CHEMISTRY

www.rsc.org/pccp

New Insights into Secondary Organic Aerosol from the Ozonolysis of α-Pinene from Combined Infrared Spectroscopy and Mass Spectrometry Measurements

Carla Kidd, Véronique Perraud and Barbara J. Finlayson-Pitts*

Department of Chemistry, University of California, Irvine, CA 92697

Revision for: Physical Chemistry Chemical Physics

August 31, 2014

*Author to whom correspondence should be addressed.

Email: bjfinlay@uci.edu; phone: (949) 824-7670; FAX (949) 824-2420

Abstract

Understanding mechanisms of formation, growth and physical properties of secondary organic aerosol (SOA) is central to predicting impacts on visibility, health and climate. It has been known for many decades that the oxidation of monoterpenes by ozone in the gas phase readily forms particles. However, the species responsible for the initial nucleation and the subsequent growth are not well established. Recent studies point to high molecular weight highly oxygenated products with extremely low vapor pressures (ELVOC, extremely low volatility organic compounds) as being responsible for the initial nucleation, with more volatile species contributing to particle growth. We report here the results of studies of SOA formed in the ozonolysis of α-pinene in air at 297 ± 2 K using atmospheric solids analysis probe (ASAP) mass spectrometry, attenuated total reflectance (ATR) Fourier transform infrared spectrometry and proton transfer reaction (PTR) mass spectrometry. Smaller particles are shown to be less volatile and have on average higher molecular mass components compared to larger particles, consistent with recent proposals regarding species responsible for the formation and growth of particles in this system. Thus the signatures of species responsible for particle development at various stages are observable even in particles of several hundred nm diameter. Pinonaldehyde and acetic acid were observed to evaporate from a film of impacted SOA at room temperature, from which the ratio of their diffusion coefficients to the square of the average film thickness, D/l^2, could be obtained. For acetic acid and pinonaldehyde, $D/l^2 = 6.8 \times 10^{-6}$ s^{-1} and 5.0×10^{-6} s^{-1} respectively, the relative magnitudes being consistent with the size difference between acetic acid and pinonaldehyde molecules. Limitations to quantifying the film thickness and hence absolute values of the diffusion coefficient are discussed and highlight a need for novel experimental methods for quantifying diffusion coefficients of organic species in SOA.

Introduction

Organic compounds are a major component of airborne particles.[1-4] A large fraction of the organic component under many circumstances is not from direct emissions, but rather is formed from low volatility products of the oxidation of volatile organic compounds (VOC) in air.[5, 6] This introduces significant complexity in developing quantitative predictive models of atmospheric particulate matter, especially given the large number of potential precursors and oxidation processes. Models have typically under-predicted SOA mass compared to measurements; even with recent improvements,[7-11] accurately predicting specific characteristics such as O:C and volatility simultaneously remains a challenge.[12] However, given the key role of particles in affecting visibility,[5, 6, 13] health[14-17] and climate,[18] a detailed understanding of such processes is critical.

There are two important aspects to the formation of particles in the atmosphere: (1) how the initial seed particles are formed and (2) how they grow.[19] It is well-established that sulfur compounds such as sulfuric and methanesulfonic acids form seed particles in the presence of ammonia, amines and water vapor.[20-27] Homogeneous nucleation of low volatility organic compounds is also a potential source of seed particles. As discussed in detail elsewhere,[28-33] for this to occur the compounds must have very low vapor pressures, recently dubbed ELVOC (extremely low VOC).[30, 34] Biogenic precursors such as α-pinene are expected to be particularly important because they have significant sources on a global basis and have structures and molecular masses such that oxidation leads to higher molecular weight, polar products that will have low volatility.

There is increasing evidence for homogeneous nucleation of large biogenic oxidation products. For example, the reaction of O_3 with α-pinene was shown using cluster chemical ionization mass spectrometry to generate gas phase oxidation products with molecular masses up to 621 amu.[35] Those with masses >430 amu were highly correlated with the formation of the smallest particles that were measured in that study (10 nm) while those with masses in the 140 - 380 amu range were correlated with larger particles, >20 nm.[35] Thermal desorption chemical ionization mass spectrometry (TDCIMS) of particles formed in this reaction showed that 40 nm particles were comprised of more carbonyl-containing compounds and low molecular weight organic acids, while there was evidence of larger, lower vapor pressure acid products such as terpenylic and pinic acids in the 10 and 20 nm particles.[36] These data suggest that particles are initially formed by homogenous nucleation of ELVOC products, while subsequent growth occurs via uptake of products having smaller masses and relatively higher vapor pressures. In a similar system, correlations between gas phase ELVOC and SOA mass were observed both in the absence and presence of inorganic seed particles[30] and ELVOC adduct ions have been identified in chamber studies and ambient air.[29] High molecular weight oligomers have also been identified by high resolution mass spectrometric techniques.[37-46] Oligomerization is proposed to occur via acid catalyzed aldol and gem-diol reactions between SOA 'monomers',[39, 42, 47, 48] generating esters, acetals and hemiacetals and/or the repeat addition of stabilized Criegee intermediates to peroxy radicals.[41]

The physical properties of SOA are still far from fully understood. While it was assumed for many years that SOA would be a relatively low viscosity liquid, a number of recent studies point

to it being a semi-solid or even glassy material under certain conditions.[32, 49-68] In this case diffusion of species will be much slower than in a liquid, which affects exchange with the gas phase and the growth mechanism for the particles. While diffusion coefficients (D) for a given viscosity (η) are often predicted through the Stokes-Einstein relationship that relates D inversely to η,[65, 69] this relationship has been shown to be inapplicable for water diffusing in highly viscous organic materials,[70, 71] which likely includes SOA under some conditions. To date there has been only one direct measurement of diffusion in α-pinene SOA, which is for pyrene incorporated into the SOA as it formed.[66]

We report here the results of studies, using a combination of experimental techniques, of the composition of particles from α-pinene ozonolysis binned into two different size ranges (250 - 500 nm and >500 nm respectively) through the use of an impactor. Even with these larger particle sizes compared to the prior studies, there is clear evidence of enhancement of higher molecular mass components in the smaller size bin and more volatile components in the larger particles. The rates at which pinonaldehyde and acetic acid diffuse out of SOA deposited on a ZnSe surface are used to estimate the likely range of magnitudes of their diffusion coefficients. These are shown to be several orders of magnitude smaller than would be expected for liquid matrices[65] and hence are consistent with SOA from this reaction being a highly viscous material, in agreement with a growing body of evidence from this[49, 50] and other laboratories.[51-59, 62-64, 66]

Experimental

SOA generation

SOA from the ozonolysis of α-pinene under dry conditions was generated in our large volume, slow flow, aerosol flow tube[72] as has been described in detail previously.[49, 50, 72] Ozone (~1 ppm) was generated by flowing high purity oxygen (Oxygen Services, Ultra High Purity, 99.993%) through a housing containing a Pen-Ray® mercury lamp (UVP, LLC, model 11SC-2) and subsequently diluting to the desired concentration. The ozone concentration was monitored by Fourier transform infrared spectroscopy (FTIR, Mattson Instruments Inc., model 10000) and a photometric O_3 analyzer (Teledyne, Model 400 E). The α-pinene ((1R)-(+)- α-pinene; Sigma Aldrich, >99%) was added to the flow tube (after purification in an alumina column) downstream of the ozone inlet and was injected into the dilution airflow to the desired gas-phase concentration (~1 ppm) using an automated syringe pump (Pump Systems Inc, model NE-1000). The clean dry dilution air was from a purge gas air generator (Parker Balston, model 75-62), passed through carbon/alumina media (Perma Pure, LLC) and an inline 0.1 μm filter (Headline Filters, DIF-N70). A scavenger for OH formed in the α-pinene-ozone reaction[5, 73] was not added in these experiments. The total flow rate in the flow tube was 34 L min^{-1} corresponding to a total residence time of 33 minutes at the sampling port at the end of the flow tube. The particle size distributions were recorded using a scanning mobility particle sizer (SMPS, TSI, model 3080 classifier and 3776 condensation particle counter). The number mode diameter was 332 nm and the mass-weighted mode was 552 nm.

ASAP-MS measurements

SOA was collected using a Sioutas impactor (SKC Inc) with ZnSe substrates operated at 9 L min^{-1}. Different stages were used to split the SOA into two size regimes of 250-500 nm and >500 nm. When collecting SOA between 250-500 nm the upper stage was greased (Dow Corning, high vacuum grease) to prevent larger particles bouncing down to the lower stage. The SOA was then physically transferred onto the tip of a glass melting point tube attached to an atmospheric solids analysis mass spectrometer probe (ASAP-MS)[74, 75] (Waters). Prior to use, the melting point tube was cleaned by baking within the source at 450 °C for at least an hour. The mass spectrometer was a LCT Premier time-of-flight mass spectrometer (Waters) and was used in positive ion mode.

The source was operated at a constant temperature of 150 °C while temperature controlled nitrogen flowed over the tip (8.3 L min^{-1}) to desorb the SOA components. The nitrogen temperature was manually ramped from 100 °C to 450 °C in a stepwise fashion in increments of 50 °C. The presence of a small container of liquid water in the source compartment resulted in the formation of H_3O^+ ions by corona discharge and these undergo proton transfer reactions with the volatilized species to form $[M+H]^+$ ions. Mass spectra and total ion signals were acquired across 100-1000 Da as a function of temperature

ATR-FTIR measurements of the SOA

SOA was sampled using a custom designed impactor[49] with a ZnSe ATR (attenuated total reflectance) crystal substrate that had been cleaned prior to use by boiling in ethanol and

dichloromethane before placing in an argon plasma for 30 min (Plasma Cleaner/Sterilizer PDC-32G, Harrick Scientific Products, Inc). The polydisperse SOA was impacted at a flow rate of 30 L min^{-1} for a total time of 5 minutes. The ATR impactor has a d_{50} cutoff diameter of 240 ± 12 nm[49] at 30 L min^{-1}, which captured most of the mass of the SOA.

IR spectra were recorded using a Nicolet™ 6700 FTIR spectrometer (Thermo Scientific). An ATR crystal was housed in a commercially available HATR (Horizontal ATR) accessory (PIKE Technologies, Madison WI). Background measurements of the clean crystal were measured for subsequent analysis. Reference spectra of adsorbed and gas phase water were also taken by flowing humid air over the clean crystal (adsorbed) and into the sampling compartment of the spectrometer (gas-phase).

Once the polydisperse SOA was impacted onto the ATR crystal, the SOA covered crystal was transferred immediately to a custom designed flow cell[76] (volume 22 cm^3) through which clean air was flowed. Infrared spectra of the SOA were recorded as single beam spectra and processed to give absorbance spectra in the form $\log_{10}(S_0/S_1)$ where S_0 represents a background relative to the spectrum of interest S_1. Spectra were recorded within ~5 min from the time of impaction and subsequent spectra were recorded every 15 minutes to monitor changes in the SOA under the flow (200 cm^3 min^{-1}) of clean dry air (Oxygen Services, Ultra High Purity) for 20 hours.

PTR-MS measurements of volatilized components

The outflow from the ATR flow cell was directed to a proton-transfer time-of-flight mass spectrometer (PTR-MS) (PTR-ToF-MS, Ionicon Analytik) to detect species evaporating from the SOA.

The PTR-MS acquisition was started prior to connecting the outflow of the ATR cell to the PTR-MS inlet via a 30 cm length of Teflon tubing. The moment of connection was taken as time t_0. Spectra were acquired at a rate of 3 scans per minute and were recorded for ~8 hours. Mass spectra were extracted using the PTR-MS TOF Viewer software (Ionicon Analytik version 1.4.0) by averaging a total of 10 individual scans starting close to t_0. Spectra after 8 hours in the clean air flow were used to determine the background. Peaks that increased significantly from this background were attributed to species evaporating from the SOA. The corresponding ion traces for the individual species were extracted after mass calibration.

Results and Discussion

Figure 1 shows typical ASAP-MS total ion signals for SOA in the smaller (250 - 500 nm; red curve) and larger (>500 nm; black curve) size bins respectively as a function of scan number/desorption temperature. The signal for the larger SOA peaked at lower temperatures compared to that for the 250 - 500 nm SOA, indicating that some of its components are more volatile. The mass spectra were averaged (MassLynx^{TM}, Waters) to give a total integrated spectrum for the temperature range 100-450 °C for each sample. Six individual samples were analyzed for each size range (250 nm and >500 nm). Figure 2 shows a typical integrated ASAP mass spectrum for the 250 - 500 nm particles (Fig 2a) and for the larger particles (Fig. 2b) (peaks

184 highlighted in purple are observed in the background and hence were not included in subsequent
185 quantitative analyses). It is clear that the smaller particles have a greater contribution to the total
186 mass spectrum from higher molecular mass components, while peaks due to smaller products of
187 this reaction are more evident in the larger particles. This is consistent with the higher volatility
188 of the larger SOA seen in Fig. 1.

189 An obvious feature of the ASAP spectra is the strong peak at $m/z = 351$. This may be due to
190 dehydrated $[M+H-H_2O]^+$ fragments of previously proposed species with molecular weight of 368
191 amu:[48, 77]

$C_{19}H_{28}O_7$ (MW 368)

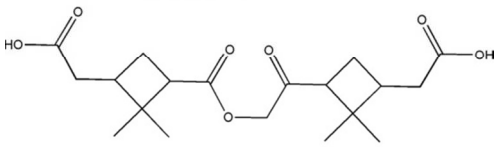

192 or

$C_{20}H_{32}O_6$ (MW 368)

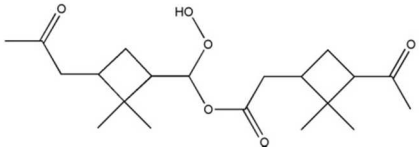

193

194 The $C_{19}H_{28}O_7$ diacid has been proposed to be formed from the reaction between pinic acid and
195 10-hydroxypinonic acid,[48] while the $C_{20}H_{32}O_6$ hydroperoxide has been proposed to result from
196 the reaction of a stabilized Criegee intermediate with pinonic acid[77] formed from the ozonolysis
197 of α-pinene. The relatively high intensity may indicate that such products are a major
198 component of the SOA or alternatively, that the sensitivity to them in ASAP-MS is higher than
199 for other components.

200

201 The integrated mass spectra were separated into mass ranges to represent SOA monomers
202 (100-200 amu), dimers (201-400 amu) and oligomers (>401 amu) as illustrated in Figure 2.
203 These boundaries are not intended to be absolute assignments of monomeric, dimeric and

oligomeric SOA components but rather to represent the mass ranges where such products are likely to be found. Figure 3 shows the fraction of the total signal that falls into each mass range for the smaller particles (red boxes) compared to the >500 nm particles (black boxes). As suggested qualitatively by the mass spectra (Fig. 2), the larger particles have a relatively greater contribution from low molecular mass components, while the smaller particles have more contribution from higher molecular masses.

Figure 4a shows a typical ATR-FTIR spectrum of polydisperse SOA immediately following impaction. For comparison, ATR spectra of pinonic acid and pinonaldehyde identified in other studies[78-93] as common products of α-pinene ozonolysis are also shown (Fig. 4 b, c). As expected, the SOA spectrum exhibits significant similarities to those for these oxygenated products. Also shown in Fig. 4d is the difference spectrum for SOA after 20 hrs under a flow of clean dry air. This spectrum is log (S_1/S_{20}) where S_1 is the first single beam spectrum after introducing the flow of air and S_{20} is that after 20 hrs, so that negative peaks represent functional groups lost from the SOA. The loss of C=O at 1695 cm^{-1} is indicative of aldehydes/ketones that have evaporated from the SOA. The loss at ~3400 cm^{-1} could in part be due to a loss of carboxylic acids although the major contributor in this region is likely water which can be taken up during the brief handling in room air and then desorbed in the air flow. The change in this region was variable from experiment to experiment.

The difference spectrum also shows that there is a loss of species with peaks at 1799 and 1768 cm^{-1} which were not obvious in the overall SOA spectrum (Fig. 4a) due to overlap with the strong 1703 cm^{-1} peak (although a shoulder can be observed). There is also a loss of a peak at

1072 cm^{-1}. Carbonyl groups with a more electronegative atom such as oxygen directly attached to the carbonyl carbon have the band due to the C=O stretching vibration shifted to higher frequencies than those for aldehydes and ketones that occurs around 1700 cm^{-1}; the same is true if the C=O is part of a strained ring.[94] In addition, if they are part of an ester or lactone, bands due to the symmetric and asymmetric C(O)-O stretch appear in the 1050 - 1370 cm^{-1} region.[94] Viable candidates for these bands in terms of α-pinene ozonolysis products include the species responsible for the *m/z* = 351 ASAP peak discussed earlier and/or terpenylic acid

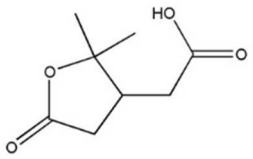

Terpenylic acid (MW 172)

which has been previously identified as a product from the attack of OH on α-pinene.[95-97] Anhydrides which have been reported in the ozonolysis of alkene self-assembled monolayers (SAMs)[98] are also a possibility.

Figure 5a shows the loss of C=O and C-H groups under a flow of clean air for 20 hrs which represents a decrease of ~20% over this time. As seen in Figure 5b, the ratio of the C=O to C-H peaks increased by ~ 10% during evaporation of the SOA, as expected if more volatile, less oxygenated products were being removed by evaporation. Zelenyuk and co-workers[62, 66] reported evaporative loss of ~ 70% of α-pinene ozonolysis SOA from individual particles up to several hundred nm in diameter over 24 hrs. In the experiments reported here, the SOA forms a film on the crystal, the concentrations of the reactants were higher and no OH scavenger was

246 added. The calculated depth of penetration of the infrared beam in the C-H stretch region at
247 2900 cm^{-1} is 0.57 μm, and at 1700 cm^{-1} is 0.98 μm.[99] As discussed below, the film is not evenly
248 spread on the crystal but its thickness in some locations may be greater than the depth of
249 penetration so that the observed evaporation (Fig. 5a) may be a lower limit. A contributing
250 factor to the discrepancies in the evaporation may also be that in the earlier studies[62, 66] there was
251 an initial rapid loss in the first few minutes during which more than ~20% of the volume fraction
252 was lost, followed by a smaller loss rate. The data in Fig. 5a were taken after the sample was
253 removed from the impactor and installed in the flow cell, which took approximately 5 min. Thus
254 a significant amount could have already evaporated by the time the first spectra were taken.
255
256 A search for gas phase products evaporating from the SOA on the ATR crystal was carried out
257 using PTR-MS to sample from the exit of the flow cell. Figure 6 shows the mass spectrum of
258 this gas stream. Although PTR-MS is a softer ionization method than electron impact, it still
259 results in significant fragmentation.[100] For example, pinonaldehyde (molecular mass 168) has a
260 weak $[M+H]^+$ peak at *m/z* = 169 but a much stronger peak at *m/z* = 151 corresponding to the
261 addition of a proton and loss of water.[87, 101-107] This makes definitive identification of gas phase
262 products in complex mixtures difficult. However, the ratio of the peaks at *m/z* = 169/151 that are
263 characteristic of pinonaldehyde is within experimental error of that reported for this compound
264 by Wisthaler et al.,[101] and the exact masses of the 151 and 169 peaks are within 25 ppm of those
265 expected for this product. Carboxylic acids such as terpenylic acid readily lose water when they
266 become protonated, which would give a peak at m/z = 155 for the $[M+H-H_2O]^+$ fragment. The
267 PTR-MS peak at 155 was bimodal and could be resolved into two peaks which are tentatively
268 assigned to: 1) terpenylic acid or norpinic acid dehydrated fragments ($[M+H-H_2O]^+$, $C_8H_{11}O_3$,

exact mass to 23 ppm) and 2) norpinonaldehyde ($[M+H]^+$, $C_9H_{15}O_2$, exact mass to 28 ppm). The strong peak at *m/z* = 61 corresponds to $[M+ H^+]$ for CH_3COOH[100] (acetic acid) which has previously been identified by PTR-MS as a gas phase product of the ozonolysis of α-pinene[87] and for which there is also evidence in the particle phase.[86]

Figure 7 shows the decays in the PTR-MS signals at *m/z* = 151 and 61 respectively as clean air flowed over the SOA on the ATR crystal. In the simplest interpretation, these reflect primarily the time for the species to diffuse through the SOA matrix. While they also include the residence time in the ATR cell and travel time to the PTR-MS, these are of the order of tens of seconds and therefore negligible in comparison to the decay times seen in Figure 7. As the *m/*z = 151 and *m/*z = 61 peaks are decaying on the timescale of hours, diffusion must be slow relative to that in liquids (where it would be effectively instantaneous on this experimental timescale),[65] suggestive of kinetic limitations in a highly viscous material. The decay of the *m/*z = 151 and *m/*z = 61 peaks, assumed to be due to pinonaldehyde and acetic acid respectively, were used to estimate the diffusion coefficients for these species in the SOA matrix.

If the generation of pinonaldehyde and acetic acid is limited only by diffusion in the SOA, then the process measured by the PTR-MS is similar to that used to determine diffusion coefficients, D, by outgassing from a sample.[108] For a thin film of thickness *l*, the time dependence of the amount of gas desorbing is an exponential of the form:[108-110]

$$\sum_{m=0}^{\infty} \frac{1}{(2m+1)^2} exp\left[-\frac{D(2m+1)^2\pi^2 t}{l^2}\right]$$

The decay of the *m/z* = 151 and 61 signals in Figure 7 were fit to exponentials of this form, from which values of D/l^2 can be derived. This approach gives $D/l^2 = 5.0 \times 10^{-6}$ s^{-1} for *m/z* = 151 and 6.8×10^{-6} s^{-1} for *m/z* = 61. The ratio of the diffusion coefficients for the species responsible for the 61 and 151 peaks in the PTR-MS data is therefore D_{61}/D_{151} =1.4. We note that the fit to the *m/z* 151 data is excellent over the entire course of the experiment out to 3 hrs. The fit to *m/z* 61 is not quite as good, which might reflect the fact that acetic acid is a sticky compound which can adsorb/desorb to surfaces in the system. If the initial data to 2 hrs for *m/z* 61 is fit by the model, the value derived for D/l^2 is 9.0×10^{-6} s^{-1} and the ratio D_{61}/D_{151} =1.8.

The Stokes-Einstein equation[69] which is often used to estimate diffusion coefficients predicts that the magnitude of the diffusion coefficient should vary inversely with the size of the diffusing molecule. The relative sizes of acetic acid and pinonaldehyde to which the peaks at 61 and 151 were assigned were calculated using the maximal estimate approach based on molar volumes.[111] The molar volume was calculated using the molecular weight of each species and the corresponding densities (a density of 1.05 g cm^{-3} was used for acetic acid and 0.83 g cm^{-3} for pinonaldehyde. In the absence of literature values for the density of pinonaldehyde, the density of nonanaldehyde was used as an approximation.). The molecular diameter σ_v was calculated according to[111]

$$\sigma_v{}^3 = \frac{6V_M}{\pi N_A}$$

where V_M is the molar volume and N_A is Avagadro's number. The resulting estimated molecular diameters are 0.56 nm and 0.85 nm respectively for acetic acid and pinonaldehyde, suggesting

the ratio of diffusion coefficients should be 1.5, in good agreement with the value of 1.4 derived from the data in Figure 7.

The outgassing of pinonaldehyde and acetic acid could reflect not only diffusion in the SOA but also potentially their generation in the SOA through secondary chemistry. If the latter is comparable to or slower than diffusion, the rate of outgassing will be a combination of the kinetics of formation in the SOA and diffusion. The fact that the ratio of D/l^2 for these two products is consistent with the ratio of their molecular sizes lends support to diffusion being the determining process in the outgassing. The Kelvin effect and capillary forces between particles have not been taken into account here because as discussed below (Fig. 8), the impacted sample forms a combination of large "spots" of many impacted particles and films of bounced particles where such effects will not be significant.

In order to derive absolute values of the diffusion coefficients, the film thickness l must be known. As shown recently in this laboratory,[49] and shown in Figure 8, the SOA forms a complex pattern on the crystal due to some particles staying directly where the particles impact initially (centerline), with others bouncing towards the periphery of the crystal (cloud). If all the SOA were collected in the spot where they initially struck and stayed there, the maximum depth of SOA would be 5 μm. It is clear from Figure 8 that this is not the case as there is significant spreading across the whole crystal. If it were spread evenly over the crystal, it would form a film of thickness ~ 150 nm.

As a result, there is no well-defined value of *l* that can be used to obtain the absolute value of the diffusion coefficients at this stage. Realistically, *l* could vary anywhere from 150 nm to a few microns. As an illustration, a film thickness of 0.75 μm would lead to values of D of 3×10^{-14} $cm^2\ s^{-1}$ and 4×10^{-14} $cm^2\ s^{-1}$ for acetic acid and pinonaldehyde respectively. Taking into account the order of magnitude or so uncertainty in *l* (which will be the major source of error in any estimate of D), this is still many orders of magnitude smaller than would be expected for a liquid matrix where diffusion coefficients of order 10^{-5}-10^{-10} $cm^2\ s^{-1}$ would be expected.[65] Abramson et al.,[66] made direct measurements of the diffusion of pyrene trapped in SOA particles during α-pinene ozonolysis by measuring the pyrene remaining in particles after exposure to activated charcoal which takes up gas phase pyrene and other volatile organics. They obtained a diffusion coefficient for pyrene of 2.5×10^{-17} $cm^2\ s^{-1}$. To our knowledge this[66] is the only direct measurement of a diffusion coefficient to date of an organic species within an SOA matrix. Their experiments were carried out with cyclohexane as an OH scavenger, which perceivably could result in SOA of a higher viscosity than in our experiments. Other factors that may contribute to the difference include that our studies involve flowing clean air over the SOA rather than depending on gas-phase diffusion from the gas-particle interface to a charcoal adsorbent at the bottom of the chamber. Diffusion coefficients may also be composition specific, depending not only on the size but also the nature of the diffusing species. The variable film thickness in our experiments limits our ability to estimate D, although no reasonable assumptions for this thickness would account for the magnitude of the differences observed. In any event, this highlights a real need for measurements of the diffusion coefficients of different organic species in SOA matrices with a variety of experimental techniques to improve our current

understanding and ability to predict condensed phase kinetic limitations on diffusion of different organic species in SOA.

Conclusions

SOA is a complex mixture of organic species which often exhibits behavior that challenges our assumptions of its composition and physical properties. Developments in high-resolution soft ionization mass spectrometry techniques have, in recent years led to the detection of previously unknown components of and precursors to SOA such as oligomers[37-46] and ELVOC.[29, 30, 35] We have shown using a combination of infrared, and gas- and particle-phase mass spectrometry that smaller particles are less volatile and have larger high molecular weight fractions than the larger particles. This is consistent with particle formation (in the absence of seed particles) by high molecular weight oligomers and ELVOC, and subsequent growth by condensation of smaller gas phase products. The evaporation rates of acetic acid and pinonaldehyde from SOA have been used to estimate the ratio of diffusion coefficients to the square of the average film thickness, D/l^2 for acetic acid and pinonaldehyde, giving $D/l^2 = 6.8 \times 10^{-6}$ s^{-1} for acetic acid and 5.0×10^{-6} s^{-1} for pinonaldehyde. Extracting absolute diffusion coefficients depends on assumptions made about the SOA film thickness. The relative magnitudes of these D/l^2 are consistent with what would be expected based on the relative sizes of acetic acid and pinonaldehyde. Reasonable estimates of the film thickness of 150 nm to a few microns put the range of diffusion coefficients in the range consistent with SOA being a highly viscous material as indicated in previous studies.[32, 49-68]

Acknowledgements

379 The authors are grateful to the National Science Foundation (NSF), grant numbers 0909227 and
380 1207112 for support of this research, and the NSF Major Research Instrumentation (MRI)
381 program (#0923323) for the PTR mass spectrometer. We also thank John Greaves of the
382 University of California, Irvine Mass Spectrometry Facility for use of the ASAP-MS and
383 technical advice.

384

References

1. J. L. Jimenez, M. R. Canagaratna, N. M. Donahue, A. S. H. Prevot, Q. Zhang, J. H. Kroll, P. F. DeCarlo, J. D. Allan, H. Coe, N. L. Ng, A. C. Aiken, K. S. Docherty, I. M. Ulbrich, A. P. Grieshop, A. L. Robinson, J. Duplissy, J. D. Smith, K. R. Wilson, V. A. Lanz, C. Hueglin, Y. L. Sun, J. Tian, A. Laaksonen, T. Raatikainen, J. Rautiainen, P. Vaattovaara, M. Ehn, M. Kulmala, J. M. Tomlinson, D. R. Collins, M. J. Cubison, J. Dunlea, J. A. Huffman, T. B. Onasch, M. R. Alfarra, P. I. Williams, K. Bower, Y. Kondo, J. Schneider, F. Drewnick, S. Borrmann, S. Weimer, K. Demerjian, D. Salcedo, L. Cottrell, R. Griffin, A. Takami, T. Miyoshi, S. Hatakeyama, A. Shimono, J. Y. Sun, Y. M. Zhang, K. Dzepina, J. R. Kimmel, D. Sueper, J. T. Jayne, S. C. Herndon, A. M. Trimborn, L. R. Williams, E. C. Wood, A. M. Middlebrook, C. E. Kolb, U. Baltensperger and D. R. Worsnop, *Science*, 2009, 326, 1525-1529.
2. J. Liggio, S. M. Li, A. Vlasenko, S. Sjostedt, R. Chang, N. Shantz, J. Abbatt, J. G. Slowik, J. W. Bottenheim, P. C. Brickell, C. Stroud and W. R. Leaitch, *Journal of Geophysical Research-Atmospheres*, 2010, 115, D21305.
3. N. L. Ng, M. R. Canagaratna, Q. Zhang, J. L. Jimenez, J. Tian, I. M. Ulbrich, J. H. Kroll, K. S. Docherty, P. S. Chhabra, R. Bahreini, S. M. Murphy, J. H. Seinfeld, L. Hildebrandt, N. M. Donahue, P. F. DeCarlo, V. A. Lanz, A. S. H. Prevot, E. Dinar, Y. Rudich and D. R. Worsnop, *Atmospheric Chemistry and Physics*, 2010, 10, 4625-4641.
4. M. Hallquist, J. C. Wenger, U. Baltensperger, Y. Rudich, D. Simpson, M. Claeys, J. Dommen, N. M. Donahue, C. George, A. H. Goldstein, J. F. Hamilton, H. Herrmann, T. Hoffmann, Y. Iinuma, M. Jang, M. E. Jenkin, J. L. Jimenez, A. Kiendler-Scharr, W. Maenhaut, G. McFiggans, T. F. Mentel, A. Monod, A. S. H. Prévôt, J. H. Seinfeld, J. D. Surratt, R. Szmigielski and J. Wildt, *Atmos Chem Phys*, 2009, 9, 5155-5236.
5. B. J. Finlayson-Pitts and J. N. Pitts, Jr., *Chemistry of the Upper and Lower Atmosphere - Theory, Experiments, and Applications*, Academic Press, San Diego, 2000.
6. J. H. Seinfeld and S. N. Pandis, *Atmospheric Chemistry from Air Pollution to Climate Change*, Wiley, 2nd edn.
7. A. G. Carlton, P. V. Bhave, S. L. Napelenok, E. D. Edney, G. Sarwar, R. W. Pinder, G. A. Pouliot and M. Houyoux, *Environmental Science & Technology*, 2010, 44, 8553-8560.
8. M. Shrivastava, J. Fast, R. Easter, W. I. Gustafson Jr, R. A. Zaveri, J. L. Jimenez, P. Saide and A. Hodzic, *Atmos Chem Phys*, 2011, 11, 6639-6662.
9. K. M. Foley, S. J. Roselle, K. W. Appel, P. V. Bhave, J. E. Pleim, T. L. Otte, R. Mathur, G. Sarwar, J. O. Young, R. C. Gilliam, C. G. Nolte, J. T. Kelly, A. B. Gilliland and J. O. Bash, *Geoscientific Model Development*, 2010, 3, 205-226.
10. A. P. Tsimpidi, V. A. Karydis, M. Zavala, W. Lei, L. Molina, I. M. Ulbrich, J. L. Jimenez and S. N. Pandis, *Atmospheric Chemistry and Physics*, 2010, 10, 525-546.
11. J. Fast, A. C. Aiken, J. Allan, L. Alexander, T. Campos, M. R. Canagaratna, E. Chapman, P. F. DeCarlo, B. de Foy, J. Gaffney, J. de Gouw, J. C. Doran, L. Emmons, A. Hodzic, S. C. Herndon, G. Huey, J. T. Jayne, J. L. Jimenez, L. Kleinman, W. Kuster, N. Marley, L. Russell, C. Ochoa, T. B. Onasch, M. Pekour, C. Song, I. M. Ulbrich, C. Warneke, D. Welsh-Bon, C. Wiedinmyer, D. R. Worsnop, X. Y. Yu and R. Zaveri, *Atmospheric Chemistry and Physics*, 2009, 9, 6191-6215.

12. K. Dzepina, C. D. Cappa, R. M. Volkamer, S. Madronich, P. F. DeCarlo, R. A. Zaveri and J. L. Jimenez, *Environmental Science & Technology*, 2011, 45, 3496-3503.
13. W. C. Hinds, *Aerosol Technology: Properties, Behavior and Measurement of Airborne Particles*, John Wiley & Sons Inc., New York, 1999.
14. J. L. Mauderly and J. C. Chow, *Inhalation Toxicology*, 2008, 20, 257-288.
15. C. A. Pope III and D. W. Dockery, *J Air & Waste Manage Assoc*, 2006, 56, 709-742.
16. M. R. Heal, P. Kumar and R. M. Harrison, *Chemical Society Reviews*, 2012, 41, 6606-6630.
17. U. Pöschl, *Angewandte Chemie International Edition*, 2005, 44, 7520-7540.
18. IPCC, *Summary for Policymakers in: Climate Change 2013: : The Physical Science Basis, Contribution of*
Working Group I to the Fifth Assessment Report of the Intergovernmental Panel on Climate Change, Cambridge University Press, Cambridge U.K., 2013.
19. R. Zhang, A. Khalizov, L. Wang, M. Hu and W. Xu, *Chemical Reviews*, 2011, 112, 1957-2011.
20. M. C. Facchini, S. Decesari, M. Rinaldi, C. Carbone, E. Finessi, M. Mircea, S. Fuzzi, F. Moretti, E. Tagliavini, D. Ceburnis and C. D. O'Dowd, *Environmental Science & Technology*, 2008, 42, 9116-9121.
21. V.-M. Kerminen, M. Aurela, R. E. Hillamo and A. Virkkula, *Tellus B*, 1997, 49, 159-171.
22. J. H. Zollner, W. A. Glasoe, B. Panta, K. K. Carlson, P. H. McMurry and D. R. Hanson, *Atmos Chem Phys*, 2012, 12, 4399-4411.
23. J. N. Smith, K. C. Barsanti, H. R. Friedli, M. Ehn, M. Kulmala, D. R. Collins, J. H. Scheckman, B. J. Williams and P. H. McMurry, *PNAS*, 2010, 107, 6634-6639.
24. J. Kirkby, J. Curtius, J. Almeida, E. Dunne, J. Duplissy, S. Ehrhart, A. Franchin, S. Gagne, L. Ickes, A. Kurten, A. Kupc, A. Metzger, F. Riccobono, L. Rondo, S. Schobesberger, G. Tsagkogeorgas, D. Wimmer, A. Amorim, F. Bianchi, M. Breitenlechner, A. David, J. Dommen, A. Downard, M. Ehn, R. C. Flagan, S. Haider, A. Hansel, D. Hauser, W. Jud, H. Junninen, F. Kreissl, A. Kvashin, A. Laaksonen, K. Lehtipalo, J. Lima, E. R. Lovejoy, V. Makhmutov, S. Mathot, J. Mikkila, P. Minginette, S. Mogo, T. Nieminen, A. Onnela, P. Pereira, T. Petaja, R. Schnitzhofer, J. H. Seinfeld, M. Sipila, Y. Stozhkov, F. Stratmann, A. Tome, J. Vanhanen, Y. Viisanen, A. Vrtala, P. E. Wagner, H. Walther, E. Weingartner, H. Wex, P. M. Winkler, K. S. Carslaw, D. R. Worsnop, U. Baltensperger and M. Kulmala, *Nature*, 2011, 476, 429-433.
25. M. L. Dawson, M. E. Varner, V. Perraud, M. J. Ezell, R. B. Gerber and B. J. Finlayson-Pitts, *Proceedings of the National Academy of Sciences*, 2012, 109, 18719-18724.
26. T. Berndt, F. Stratmann, M. Sipilä, J. Vanhanen, T. Petäjä, J. Mikkilä, A. Grüner, G. Spindler, R. Lee Mauldin Iii, J. Curtius, M. Kulmala and J. Heintzenberg, *Atmos Chem Phys*, 2010, 10, 7101-7116.
27. S. Angelino, D. T. Suess and K. A. Prather, *Environmental Science & Technology*, 2001, 35, 3130-3138.
28. A. H. Goldstein and I. E. Galbally, *Environmental Science and Technology*, 2007, DOI: citeulike-article-id:1283626, 1515-1521.
29. M. Ehn, E. Kleist, H. Junninen, T. Petäjä, G. Lönn, S. Schobesberger, M. Dal Maso, A. Trimborn, M. Kulmala, D. R. Worsnop, A. Wahner, J. Wildt and T. F. Mentel, *Atmos Chem Phys*, 2012, 12, 5113-5127.

30. M. Ehn, J. A. Thornton, E. Kleist, M. Sipilä, H. Junninen, I. Pullinen, M. Springer, F. Rubach, R. Tillmann, B. Lee, F. Lopez-Hilfiker, S. Andres, I.-H. Acir, M. Rissanen, T. Jokinen, S. Schobesberger, J. Kangasluoma, J. Kontkanen, T. Nieminen, T. Kurtén, L. B. Nielsen, S. Jørgensen, H. G. Kjaergaard, M. Canagaratna, M. D. Maso, T. Berndt, T. Petäjä, A. Wahner, V.-M. Kerminen, M. Kulmala, D. R. Worsnop, J. Wildt and T. F. Mentel, *Nature*, 2014, 506, 476-479.
31. S. K. Friedlander, *Smoke and Dust Haze*, Oxford University Press, New York, 2nd edn., 2000.
32. I. Riipinen, J. R. Pierce, T. Yli-Juuti, T. Nieminen, S. Häkkinen, M. Ehn, H. Junninen, K. Lehtipalo, T. Petäjä, J. Slowik, R. Chang, N. C. Shantz, J. Abbatt, W. R. Leaitch, V. M. Kerminen, D. R. Worsnop, S. N. Pandis, N. M. Donahue and M. Kulmala, *Atmos Chem Phys*, 2011, 11, 3865-3878.
33. M. Shrivastava, A. Zelenyuk, D. Imre, R. Easter, J. Beranek, R. A. Zaveri and J. Fast, *Journal of Geophysical Research: Atmospheres*, 2013, 118, 3328-3342.
34. N. M. Donahue, J. H. Kroll, S. N. Pandis and A. L. Robinson, *Atmos Chem Phys*, 2012, 12, 615-634.
35. J. Zhao, J. Ortega, M. Chen, P. H. McMurry and J. N. Smith, *Atmos Chem Phys*, 2013, 13, 7631-7644.
36. P. M. Winkler, J. Ortega, T. Karl, L. Cappellin, H. R. Friedli, K. Barsanti, P. H. McMurry and J. N. Smith, *Geophys Res Lett*, 2012, 39, L20815.
37. M. Kalberer, D. Paulsen, M. Sax, M. Steinbacher, J. Dommen, A. S. H. Prevot, R. Fisseha, E. Weingartner, V. Frankevich, R. Zenobi and U. Baltensperger, *Science*, 2004, 303, 1659-1662.
38. M. P. Tolocka, M. Jang, J. M. Ginter, F. J. Cox, R. M. Kamens and M. V. Johnston, *Environmental Science & Technology*, 2004, 38, 1428-1434.
39. S. Gao, N. L. Ng, M. Keywood, V. Varutbangkul, R. Bahreini, A. Nenes, J. He, K. Y. Yoo, J. L. Beauchamp, R. P. Hodyss, R. C. Flagan and J. H. Seinfeld, *Environmental Science & Technology*, 2004, 38, 6582-6589.
40. D. S. Gross, M. E. Gälli, M. Kalberer, A. S. H. Prevot, J. Dommen, M. R. Alfarra, J. Duplissy, K. Gaeggeler, A. Gascho, A. Metzger and U. Baltensperger, *Analytical Chemistry*, 2006, 78, 2130-2137.
41. A. Sadezky, R. Winterhalter, B. Kanawati, A. Rompp, B. Spengler, A. Mellouki, G. LeBras, P. Chaimbault and G. K. Moortgat, *Atmos Chem Phys*, 2008, 8, 2667-2669.
42. W. A. Hall and M. V. Johnston, *Journal of The American Society for Mass Spectrometry*, 2012, 23, 1097-1108.
43. W. A. Hall and M. V. Johnston, *Aerosol Science and Technology*, 2011, 45, 37-45.
44. J. F. Hamilton, A. C. Lewis, T. J. Carey and J. C. Wenger, *Analytical Chemistry*, 2008, 80, 474-480.
45. L. Müller, M. C. Reinnig, J. Warnke and T. Hoffmann, *Atmos Chem Phys*, 2008, 8, 1423-1433.
46. K. J. Heaton, M. A. Dreyfus, S. Wang and M. V. Johnston, *Environmental Science & Technology*, 2007, 41, 6129-6136.
47. M. Jang, N. M. Czoschke, S. Lee and R. M. Kamens, *Science*, 2002, 298, 814-817.
48. F. Yasmeen, R. Vermeylen, N. Maurin, E. Perraudin, J.-F. Doussin and M. Claeys, *Environmental Chemistry*, 2012, 9, 236-246.

49. C. Kidd, V. Perraud, L. M. Wingen and B. J. Finlayson-Pitts, *Proceedings of the National Academy of Sciences*, 2014, DOI: 10.1073/pnas.1322558111, 7552–7557.
50. V. Perraud, E. A. Bruns, M. J. Ezell, S. N. Johnson, Y. Yu, M. L. Alexander, A. Zelenyuk, D. Imre, W. L. Chang, D. Dabdub, J. F. Pankow and B. J. Finlayson-Pitts, *Proceedings of the National Academy of Sciences*, 2012, 109, 2836-2841.
51. T. D. Vaden, C. Song, R. A. Zaveri, D. Imre and A. Zelenyuk, *Proceedings of the National Academy of Sciences*, 2010, DOI: 10.1073/pnas.0911206107, 6658–6663.
52. C. D. Cappa and K. R. Wilson, *Atmos Chem Phys*, 2011, 11, 1895-1911.
53. M. Kuwata and S. T. Martin, *Proceedings of the National Academy of Sciences*, 2012, DOI: 10.1073/pnas.1209071109, 17354–17359.
54. L. Renbaum-Wolff, J. W. Grayson, A. P. Bateman, M. Kuwata, M. Sellier, B. J. Murray, J. E. Shilling, S. T. Martin and A. K. Bertram, *Proceedings of the National Academy of Sciences*, 2013, DOI: 10.1073/pnas.1219548110, 8014-8019.
55. E. Saukko, H. Kuuluvainen and A. Virtanen, *Atmospheric Measurement Techniques*, 2012, 5, 259-265.
56. A. Virtanen, J. Kannosto, H. Kuuluvainen, A. Arffman, J. Joutsensaari, E. Saukko, L. Hao, P. Yli-Pirila, P. Tiitta, J. K. Holopainen, J. Keskinen, D. R. Worsnop, J. N. Smith and A. Laaksonen, *Atmospheric Chemistry and Physics*, 2011, 11, 8759-8766.
57. R. E. O'Brien, A. Neu, S. A. Epstein, A. C. MacMillan, B. Wang, S. T. Kelly, S. A. Nizkorodov, A. Laskin, R. C. Moffet and M. K. Gilles, *Geophysical Research Letters*, 2014, 41, 4347–4353.
58. M. Shiraiwa, L. D. Yee, K. A. Schilling, C. L. Loza, J. S. Craven, A. Zuend, P. J. Ziemann and J. H. Seinfeld, *Proceedings of the National Academy of Sciences of the United States of America*, 2013, 110, 11746-11750.
59. M. Shiraiwa and J. H. Seinfeld, *Geophysical Research Letters*, 2012, 39, L24801.
60. C. D. Cappa and J. L. Jimenez, *Atmos Chem Phys*, 2010, 10, 5409-5424.
61. L. I. Kleinman, S. R. Springston, J. Wang, P. H. Daum, Y. N. Lee, L. J. Nunnermacker, G. I. Senum, J. Weinstein-Lloyd, M. L. Alexander, J. Hubbe, J. Ortega, R. A. Zaveri, M. R. Canagaratna and J. Jayne, *Atmos Chem Phys*, 2009, 9, 4261-4278.
62. T. D. Vaden, D. Imre, J. Beranek, M. Shrivastava and A. Zelenyuk, *Proceedings of the National Academy of Sciences of the United States of America*, 2011, 108, 2190-2195.
63. E. Saukko, A. T. Lambe, P. Massoli, T. Koop, J. P. Wright, D. R. Croasdale, D. A. Pedernera, T. B. Onasch, A. Laaksonen, P. Davidovits, D. R. Worsnop and A. Virtanen, *Atmos Chem Phys*, 2012, 12, 7517-7529.
64. A. Virtanen, J. Joutsensaari, T. Koop, J. Kannosto, P. Yli-Pirilä, J. Leskinen, J. M. Mäkelä, J. K. Holopainen, U. Pöschl, M. Kulmala, D. R. Worsnop and A. Laaksonen, *Nature*, 2010, 467, 824-827.
65. M. Shiraiwa, M. Ammann, T. Koop and U. Poschl, *Proceedings of the National Academy of Sciences of the United States of America*, 2011, 108, 11003-11008.
66. E. Abramson, D. Imre, J. Beránek, J. Wilson and A. Zelenyuk, *Physical chemistry chemical physics: PCCP*, 2013, 15, 2983-2991.
67. T. Koop, J. Bookhold, M. Shiraiwa and U. Poschl, *Physical Chemistry Chemical Physics*, 2011, 13, 19238-19255.
68. B. Zobrist, C. Marcolli, D. A. Pedernera and T. Koop, *Atmos Chem Phys*, 2008, 8, 5221-5244.

69. K. J. Laidler and J. H. Meiser, *Physical Chemistry*, Longman, 1982.
70. R. M. Power, S. H. Simpson, J. P. Reid and A. J. Hudson, *Chemical Science*, 2013, 4, 2597-2604.
71. H. C. Price, B. J. Murray, J. Mattsson, D. O'Sullivan, T. W. Wilson, K. J. Baustian and L. G. Benning, *Atmos Chem Phys*, 2014, 14, 3817-3830.
72. M. J. Ezell, S. N. Johnson, Y. Yu, V. Perraud, E. A. Bruns, M. L. Alexander, A. Zelenyuk, D. Dabdub and B. J. Finlayson-Pitts, *Aerosol Science and Technology*, 2010, 44, 329-338.
73. R. Atkinson, S. M. Aschmann, J. Arey and B. Shorees, *Journal of Geophysical Research: Atmospheres*, 1992, 97, 6065-6073.
74. E. A. Bruns, V. r. Perraud, J. Greaves and B. J. Finlayson-Pitts, *Analytical Chemistry*, 2010, 82, 5922-5927.
75. E. A. Bruns, J. Greaves and B. J. Finlayson-Pitts, *The Journal of Physical Chemistry A*, 2012, 116, 5900-5909.
76. S. G. Moussa and B. J. Finlayson-Pitts, *Physical Chemistry Chemical Physics*, 2010, 12, 9419–9428.
77. S. Lee and R. M. Kamens, *Atmospheric Environment*, 2005, 39, 6822-6832.
78. T. S. Christoffersen, J. Hjorth, O. Horie, N. R. Jensen, D. Kotzias, L. L. Molander, P. Neeb, L. Ruppert, R. Winterhalter, A. Virkkula, K. Wirtz and B. R. Larsen, *Atmospheric Environment*, 1998, 32, 1657-1661.
79. M. Glasius, M. Duane and B. R. Larsen, *Journal of Chromatography A*, 1999, 833, 121-135.
80. M. Glasius, M. Lahaniati, A. Calogirou, D. Di Bella, N. R. Jensen, J. Hjorth, D. Kotzias and B. R. Larsen, *Environmental Science & Technology*, 2000, 34, 1001-1010.
81. S. Hatakeyama, K. Izumi, T. Fukuyama and H. Akimoto, *Journal of Geophysical Research: Atmospheres*, 1989, 94, 13013-13024.
82. T. Hoffmann, J. Odum, F. Bowman, D. Collins, D. Klockow, R. Flagan and J. Seinfeld, *Journal of Atmospheric Chemistry*, 1997, 26, 189-222.
83. T. Hoffmann, R. Bandur, U. Marggraf and M. Linscheid, *Journal of Geophysical Research: Atmospheres*, 1998, 103, 25569-25578.
84. J. Yu, R. C. Flagan and J. H. Seinfeld, *Environmental Science & Technology*, 1998, 32, 2357-2370.
85. J. Yu, D. Cocker, III, R. Griffin, R. Flagan and J. Seinfeld, *Journal of Atmospheric Chemistry*, 1999, 34, 207-258.
86. S. Koch, R. Winterhalter, E. Uherek, A. Kolloff, P. Neeb and G. K. Moortgat, *Atmospheric Environment*, 2000, 34, 4031-4042.
87. A. Lee, A. H. Goldstein, J. H. Kroll, N. L. Ng, V. Varutbangkul, R. C. Flagan and J. H. Seinfeld, *Journal of Geophysical Research: Atmospheres*, 2006, 111, D17305.
88. R. Winterhalter, R. Van Dingenen, B. R. Larsen, N. R. Jensen and J. Hjorth, *Atmos Chem Phys Discuss*, 2003, 3, 1-39.
89. M. Jang and R. M. Kamens, *Atmospheric Environment*, 1999, 33, 459-474.
90. J. Warnke, R. Bandur and T. Hoffmann, *Analytical and Bioanalytical Chemistry*, 2006, 385, 34-45.
91. Y. Iinuma, O. Böge, T. Gnauk and H. Herrmann, *Atmospheric Environment*, 2004, 38, 761-773.

92. Y. Iinuma, O. Boge, Y. Miao, B. Sierau, T. Gnauk and H. Herrmann, *Faraday Discuss*, 2005, 130, 279-294.
93. M. Jaoui, T. E. Kleindienst, M. Lewandowski, J. H. Offenberg and E. O. Edney, *Environmental Science & Technology*, 2005, 39, 5661-5673.
94. G. Socrates, *Infrared and Raman Characteristic Group Frequencies: Tables and Charts*, John Wiley & Sons, West Sussex, 2007.
95. F. Yasmeen, R. Vermeylen, R. Szmigielski, Y. Iinuma, O. Böge, H. Herrmann, W. Maenhaut and M. Claeys, *Atmospheric Chemistry and Physics*, 2010, 10, 9383-9392.
96. M. Claeys, Y. Iinuma, R. Szmigielski, J. D. Surratt, F. Blockhuys, C. Van Alsenoy, O. Böge, B. Sierau, Y. Gómez-González, R. Vermeylen, P. Van der Veken, M. Shahgholi, A. W. H. Chan, H. Herrmann, J. H. Seinfeld and W. Maenhaut, *Environmental Science & Technology*, 2009, 43, 6976-6982.
97. A. Kahnt, Y. Iinuma, F. Blockhuys, A. Mutzel, R. Vermeylen, T. E. Kleindienst, M. Jaoui, J. H. Offenberg, M. Lewandowski, O. Böge, H. Herrmann, W. Maenhaut and M. Claeys, *Environmental Science & Technology*, 2014, 48, 4901-4908.
98. L. R. Fiegland, M. McCorn Saint Fleur and J. R. Morris, *Langmuir*, 2005, 21, 2660-2661.
99. N. J. Harrick, *Internal Reflection Spectroscopy*, John Wiley & Sons, 1967.
100. J. de Gouw and C. Warneke, *Mass Spectrometry Reviews*, 2007, 26, 223-257.
101. A. Wisthaler, N. R. Jensen, R. Winterhalter, W. Lindinger and J. Hjorth, *Atmospheric Environment*, 2001, 35, 6181-6191.
102. B. Warscheid and T. Hoffmann, *Atmospheric Environment*, 2001, 35, 2927-2940.
103. P. Barmet, J. Dommen, P. F. DeCarlo, T. Tritscher, A. P. Praplan, S. M. Platt, A. S. H. Prévôt, N. M. Donahue and U. Baltensperger, *Atmos Meas Tech*, 2012, 5, 647-656.
104. S. Kim, T. Karl, A. Guenther, G. Tyndall, J. Orlando, P. Harley, R. Rasmussen and E. Apel, *Atmos Chem Phys*, 2010, 10, 1759-1771.
105. K. P. Wyche, A. C. Ryan, C. N. Hewitt, M. R. Alfarra, G. McFiggans, T. Carr, P. S. Monks, K. L. Smallbone, G. Capes, J. F. Hamilton, T. A. M. Pugh and A. R. MacKenzie, *Atmos Chem Phys Discuss*, 2014, 14, 14291-14349.
106. Y. Yu, M. J. Ezell, A. Zelenyuk, D. Imre, L. Alexander, J. Ortega, B. D'Anna, C. W. Harmon, S. N. Johnson and B. J. Finlayson-Pitts, *Atmospheric Environment*, 2008, 42, 5044-5060.
107. M. Camredon, J. F. Hamilton, M. S. Alam, K. P. Wyche, T. Carr, I. R. White, P. S. Monks, A. R. Rickard and W. J. Bloss, *Atmos Chem Phys*, 2010, 10, 2893-2917.
108. J. E. Shelby, *Handbook of Gas Diffusion in Solids and Melts*, ASM International, Materials Park, OH, 1996.
109. R. M. Barrer, *Diffusion In and Through Solids*, Cambridge University Press, Cambridge, England, 1941.
110. J. Crank, *The Mathematics of Diffusion*, Oxford University Press, London, England, 1964.
111. Y. Marcus, *Journal of Physical Organic Chemistry*, 2003, 16, 398-408.

Figures

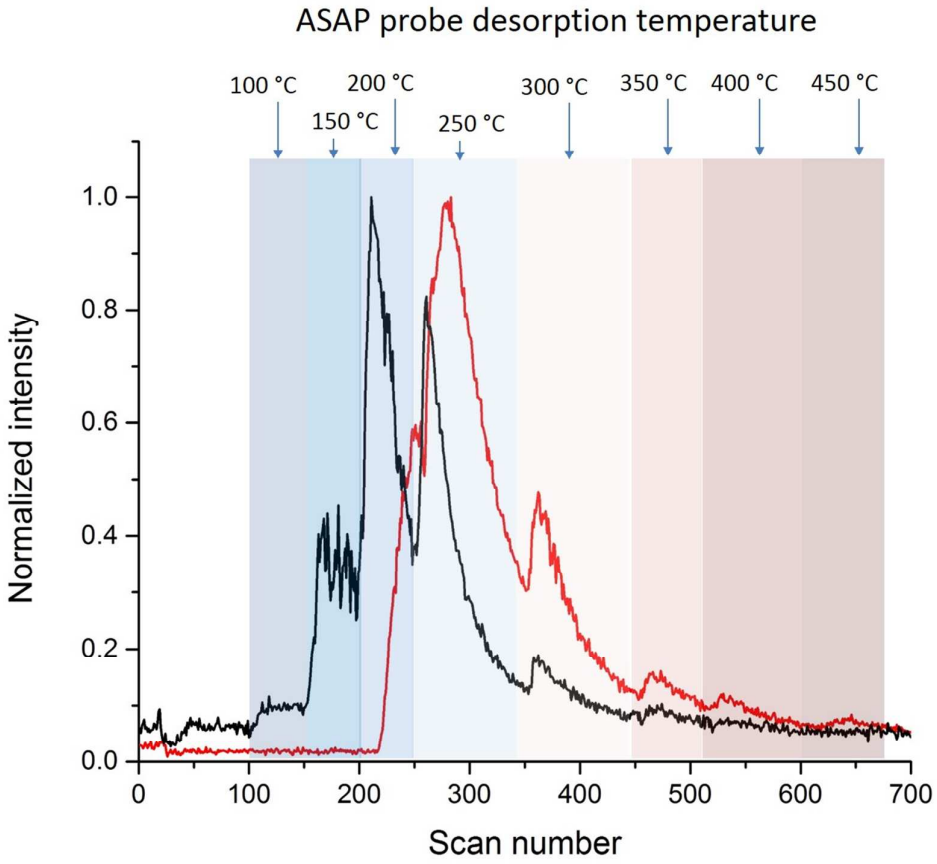

Figure 1: Total ion signal (TIS) for ASAP-MS analysis of SOA from the ozonolysis of α-pinene as a function of scan number and corresponding ASAP probe desorption temperature. The SOA was separated into fractions by particle size of 250-500 nm (red) and >500 nm (black) by impaction prior to analysis. TIS have been peak normalized for comparison.

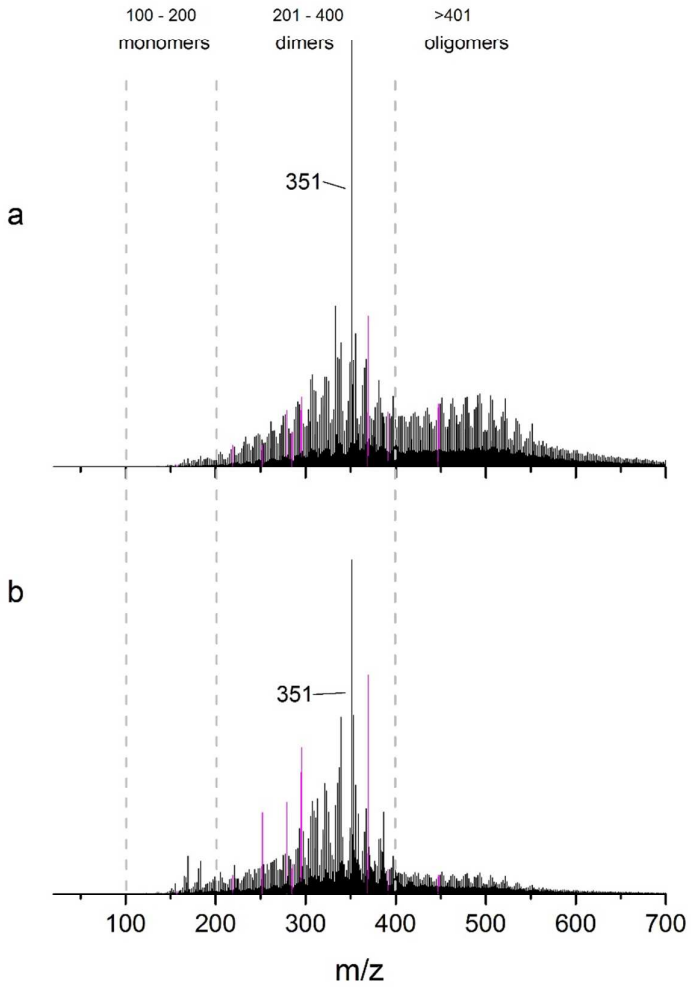

Figure 2: Typical ASAP mass spectra of SOA from the ozonolysis of α-pinene separated into size fractions of (a) 250-500 nm particles and (b) >500 nm particles by a Sioutas impactor prior to analysis. The spectra have been normalized to the peak at an *m/z* of 351. The peaks highlighted in purple are observed in background spectra and are not included in quantitative analyses of the spectra. Dashed lines represent the boundaries for the quantitative analysis to assign to monomers, dimers, and oligomers. These boundaries are for illustrative purposes only.

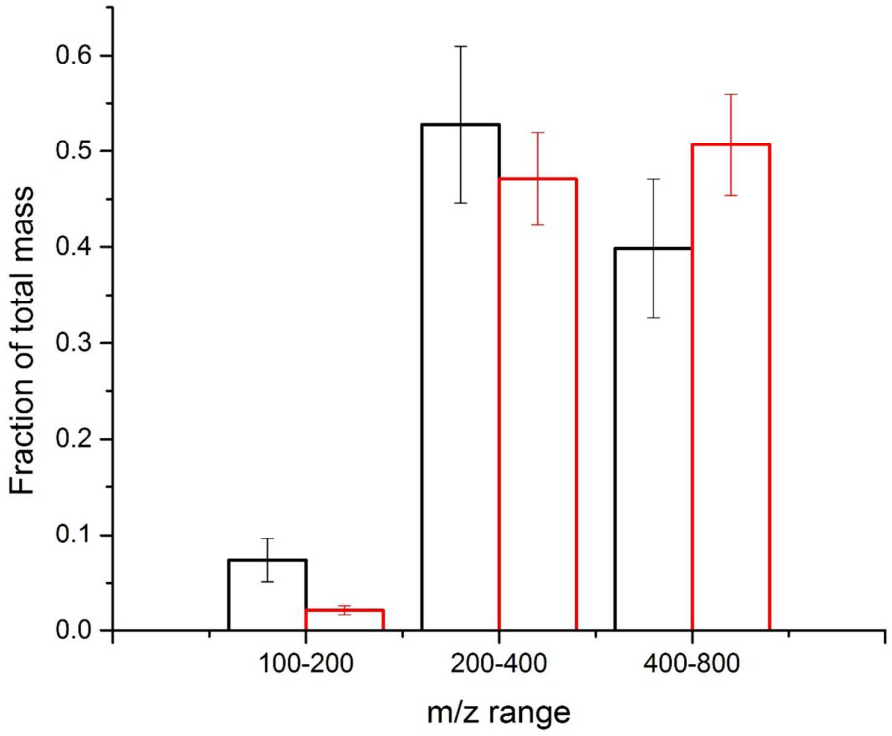

Figure 3: Fraction of the total signal detected by ASAP-MS as a function of *m/z* range for SOA from the ozonolysis of α-pinene. The SOA was separated into ranges by particle size of 250-500 nm (red) and >500 nm (black) by impaction prior to analysis. Six individual spectra were analysed for each size bin and the fractions represent the average of the six measurements and associated 1σ error. Contributions from contaminant peaks, highlighted in purple in Figure 2, were subtracted from the integrals before calculating the relative fractions. The contribution from contaminants was of order 2-4% of the total signal detected.

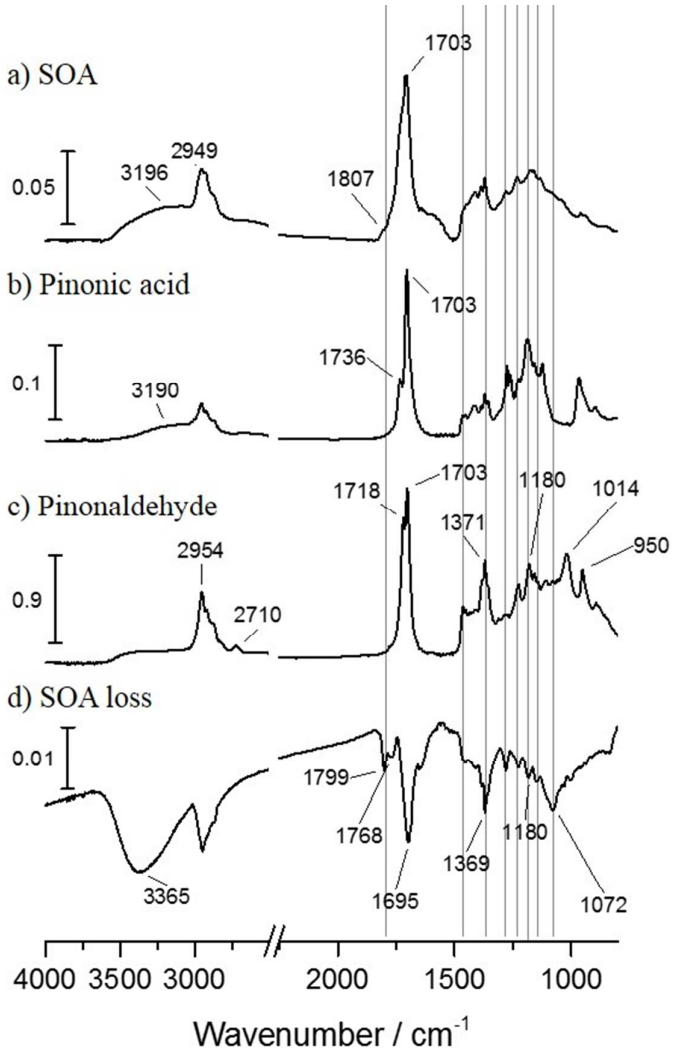

Figure 4: a) ATR-FTIR spectra of SOA from the ozonolysis of α-pinene. Absorbance (y axis) is $\log_{10}(S_0/S_1)$ where S_0 is the single beam spectrum of a clean crystal and S_1 the spectrum of the SOA covered crystal immediately following impaction. Contributions from gas-phase water have been subtracted; b) and c) are reference spectra of authentic samples of pinonic acid and pinonaldehye. d) is the difference spectrum for SOA after 20 hrs of clean air flow over the sample. This spectrum is $\log_{10}(S_1/S_{20})$ where S_1 is the spectrum of the SOA covered crystal immediately following impaction and S_{20} is that after 20 hrs of clean air flow. Grey lines are to aid visual comparison between spectra.

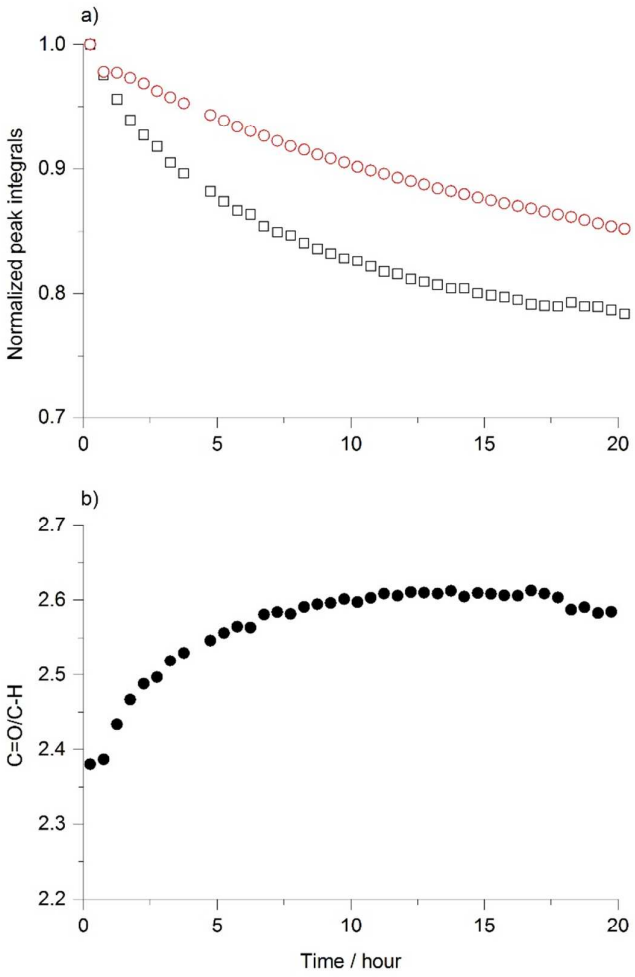

Figure 5: (a) Normalized (at t=0) integrated C-H peak (open black squares) and C=O peak (open red circles) for SOA as a function of time under a flow of clean air. (b) Ratio of C=O to C-H of peak integrals as a function of time under a flow of clean dry air for SOA from the ozonolysis of α-pinene. The C=O peak was the integrated area from 1658-1850 cm^{-1}, but the peak at ~ 1700 cm^{-1} dominates the signal. That for C-H was the integral from 2810 - 3050 cm^{-1}.

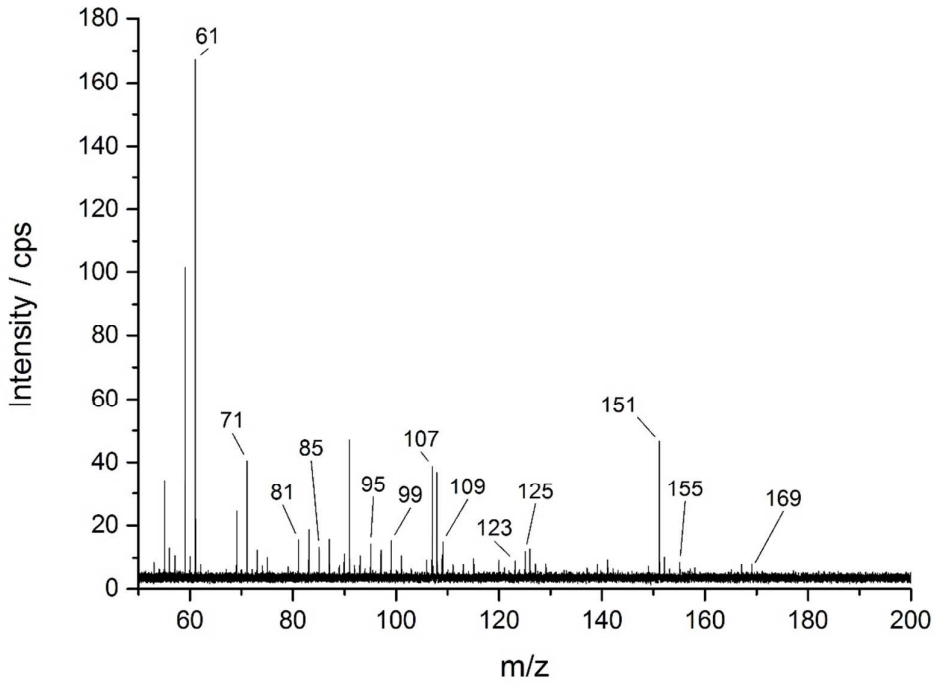

Figure 6: PTR-MS spectrum of air flowing over SOA from α-pinene ozonolysis. Spectrum is an average of 10 individual scans and is shown without background subtraction. Labelled peaks are those that were observable above the background. All other peaks in were present in background also and are therefore not assigned to species evaporating from SOA.

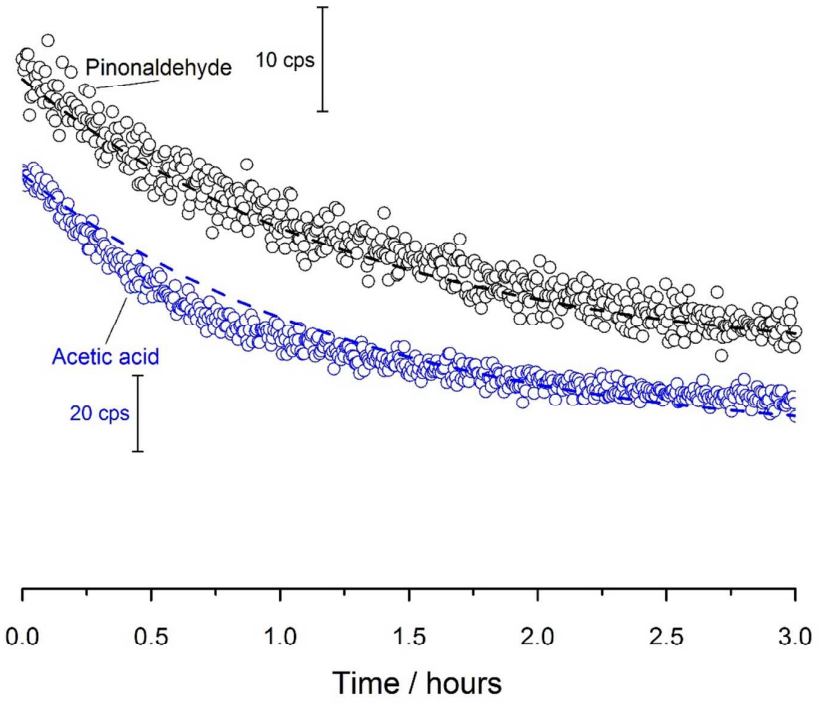

Figure 7: PTR-MS time traces for *m/z* 151 (black open circles) assumed to be acetic acid, and *m/z* 61 (blue open circles) assumed to be pinonaldehyde, extracted from PTR-MS spectra of air flowing over SOA. The vertical bars give the scale for the signal intensity for the Y-axis in counts per second (cps). Dashed lines are fits to modelled diffusion assuming a D/l^2 of 5.0×10^{-6} s^{-1} for *m/z* 151 and D/l^2 of 6.8×10^{-6} s^{-1} for *m/z* 61 as described in the text.

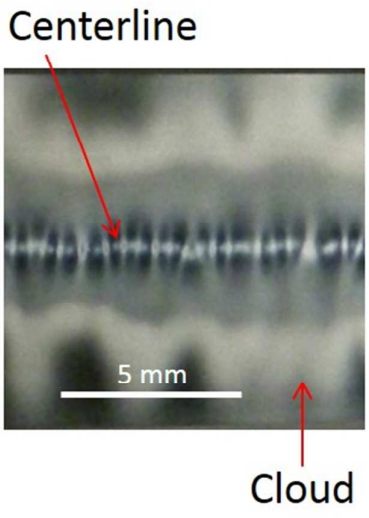

Figure 8: Digital photograph of SOA impacted onto a Ge ATR crystal (scale bar = 5 mm) at 30 L min^{-1} for 5 minutes. Ge was used as ZnSe does not provide the contrast needed to photograph the SOA. The ATR crystal is 8×1 cm (length by width) thus the photograph represents the full width of an SOA coated ATR crystal and a 1 cm portion of its length. The light color is impacted SOA and the dark colour is the Ge substrate. SOA particles impact initially at the centerline and may subsequently bounce forming the uneven coverage observed.